Molecular Capture in Protein Nanotubes

Xue Qu[†] and Teruyuki Komatsu[†,‡,*]

[†]Research Institute for Science and Engineering, Waseda University, 3-4-1 Okubo, Shinjuku-ku, Tokyo 169-8555, Japan, and [‡]PRESTO, Japan Science and Technology Agency (JST), 4-1-8 Honcho, Kawaguchi-shi, Saitama 332-0012, Japan

ABSTRACT We describe molecular capturing properties of protein nanotubes with a controllable ligand binding affinity and size selectivity. These practical biocylinders were prepared using an alternating layer-by-layer (LbL) assembly of protein and oppositely charged poly(amino acid) into the nanoporous polycarbonate (PC) membrane (pore diameter, 400 nm), with subsequent dissolution of the template. The tube wall typically comprises six layers of poly-L-arginine (PLA) and human serum albumin (HSA) [$(PLA/HSA)_3$]. Use of high molecular weight PLA (M_w = *ca.* 70 000) yielded robust nanotubes, which are available as lyophilized powder. The $(PLA/HSA)_3$ nanotubes swelled considerably in water, although the outer diameter was almost unaltered. Uranyl ion, 3,3′-diethylthiacarbocyanine iodide, and zinc(II) protoporphyrin IX (ZnPP) were bound to the HSA component in the cylinder wall. Similar nanotubes comprising recombinant HSA mutant [rHSA(His)], which has a strong binding affinity for ZnPP, captured this ligand more tightly. Furthermore, addition of excess myristic acid released ZnPP from the tubes through a ligand replacement reaction. The hybrid nanotubes bearing a single avidin layer as an internal surface captured FITC-biotin efficiently. Biotin-labeled nanoparticles are also incorporated into the tubes when their particle size is sufficiently small to enter the pores. Subsequent TEM observation revealed a line of loaded nanoparticles (100 nm) in the one-dimensional space interior.

KEYWORDS: protein · nanotube · template · assembly · human serum albumin

There is much current interest in synthesizing cylindrical hollow structures by template synthesis using a nanoporous membrane.[1−3] In particular, the alternate layer-by-layer (LbL) assembly technique, which involves multilayer build up onto the channel surface, enables creation of various kinds of nanotubes composed of many combinations of materials.[4−10] A typical example is polymer cylinders made of a pair of oppositely charged synthetic polyelectrolytes that interact *via* electrostatic interaction.[11−17] The outer diameter, length, and composition of the cylinder wall can be modulated according to the pore diameter, membrane thickness, and the particular combination of polymers used for their production. Proteins are naturally occurring polyelectrolytes showing versatile biochemical reactivity. Artificial mutants having unique functional responses that are never seen in nature may also be produced using genetic engineering. Consequently, protein nanotubes have attracted considerable attention because of their potential biomedical applications, such as drug delivery, biomolecular separation, and enzymatic reactions.[18−24] Nanotubes present several advantages over nanospheres. First, nanotubes can possess different interior and exterior surfaces independently. It is therefore possible to construct a one-dimensional space interior for specific reactions and a biocompatible surface exterior that can be tailored to target specific tissues or to respond to particular stimuli. Second, nanotubes have open-end terminals, which may be useful for delivery applications. Large quantities of guest molecules can be readily loaded and released without structural change. Third, nanotubes can have long circulation persistence *in vivo*. Discher *et al.* reported that polymer cylinders of 8 μm length remained in the bloodstream of rats up to 1 week after intravenous injection, about 10 times longer than spherical particles of the same composition.[25] Nevertheless, few reports describe smart nanotubes composed of natural or recombinant proteins. Martin *et al.* first reported the synthesis of glucose oxidase nanotubes using a hard porous Al_2O_3 membrane. Each protein layer was cross-linked by glutaraldehyde, and the template was dissolved by chemical etching with 5% phosphoric acid.[18] Unfortunately, many tubes were broken during the membrane dissolution process. Li *et al.* prepared $(cytochrome\ c/PSS)_5$ nanotubes [PSS: poly(styrenesulfonate)] using an Al_2O_3 membrane, which should be dissolved also in acidic conditions.[22] We recently demonstrated the synthesis of several nanotubes composed of a combination of negatively charged protein and positively charged polycation,

*Address correspondence to teruyuki@waseda.jp.

Received for review October 23, 2009 and accepted December 11, 2009.

Published online December 18, 2009.
10.1021/nn901474y

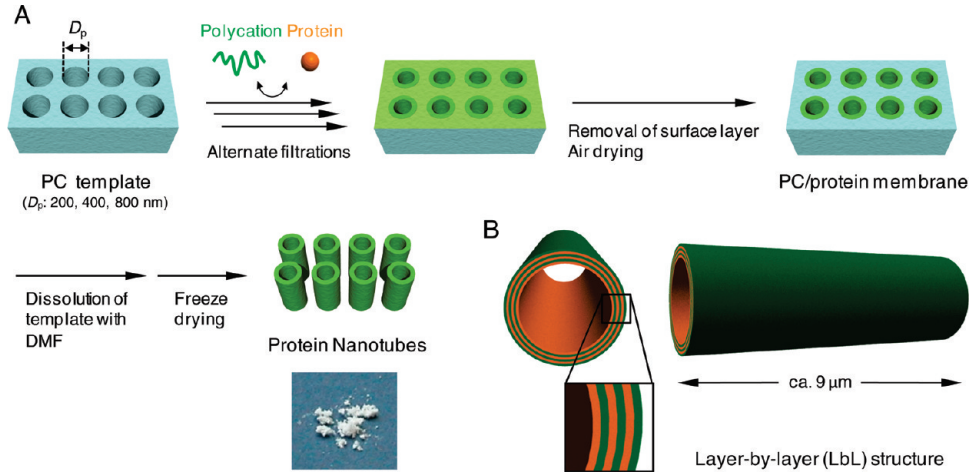

Scheme 1. (A) Synthesis of protein nanotubes by LbL deposition technique using nanoporous PC membrane. (B) Schematic illustration of $(PLA/HSA)_3$ nanotube prepared using a 400 nm porous PC template.

for example, human serum albumin (HSA) and poly-L-arginine (PLA), using a porous polycarbonate (PC) membrane.[23] The template can be dissolved rapidly in CH_2Cl_2, and the liberated tubules are collected by vacuum filtration. However, this extraction process results in significant physical deformation of the nanotubes, which appear crumpled on the filter surface. In this paper, we describe a new procedure in which the tubes were carefully extracted from the PC template using *N*,*N*-dimethylformamide (DMF) and rapidly freeze-dried to yield a lyophilized powder that was readily dispersed in aqueous solution. Using this method, we generated several different HSA-based nanotubes and characterized the molecule-capturing capabilities of their cylindrical walls and one-dimensional pore space interiors. Our results constitute a new chemistry of protein nanotubes that may serve as bioseparation devices with a controllable ligand binding affinity and size selectivity.

RESULTS AND DISCUSSION

Extraction of Protein Nanotubes from PC Template. We previously demonstrated the primary synthesis of protein nanotubes using the LbL deposition technique with a track-etched PC membrane.[23] Typically, three cycles of injection of the PLA solution followed by the HSA solution into the nanoporous membrane (pore diameter, D_p = 400 nm) yielded uniform $(PLA/HSA)_3$ cylinders after dissolution of the PC template with CH_2Cl_2. The released nanotubes were filtered carefully under reduced pressure using tetrafluoroethylene membrane (100 nm pore size). However, this procedure is problematic for two reasons. First, the tubes are not sufficiently strong to survive vacuum filtration and air-drying, so many of them become crumpled and lose their tubular structure. Second, it is difficult to disperse the nanotubes into water since they tended to adhere to the top of the fluorinated membrane. To develop these promising biocylinders as a novel advanced material, we must extract them without deformation from the PC framework. Herein, we present two important techniques used for extraction of the cylindrical cores from the channels (Scheme 1).

First, the etching solvent was changed to DMF. The tube damage in this polar amide solvent was apparently negligible compared to that in other possible reagents. Second, PLA with a high molecular weight (M_w = *ca.* 70 000) was exploited as an electrostatic glue for the mutual cohesion of the albumin protein layers. This provided more robust nanotubes compared to those obtained using a PLA with lower molecular weight (M_w = 25 000−70 000). Third, as the most important alteration, the liberated protein nanotubes were quickly freeze-dried, yielding lyophilized powder as many pieces of the thin film (~4 mm^2). Surprisingly, these pieces were composed of beautiful arrays of $(PLA/HSA)_3$ nanotubes, with an outer diameter of 407 ± 13 nm and wall thickness of 50 ± 4 nm, as revealed by SEM observations (Figure 1A−D). When the PC/protein membrane was immersed into the DMF solution, the porous PC support disappeared immediately and the neighboring nanotubes caused stacking, thereby forming such a highly ordered arrangement. The maximum length of the tubules (*ca.* 9 μm) corresponded to the PC membrane pore depth (Figure 1A,D). Shorter or forked nanotubes were also present because the template channels are sometimes not continuous throughout the film. We have successfully developed efficient methods to extract protein nanotubes from the PC membrane. This procedure is likely to be applicable to preparations of any cylindrical hollow structures composed of various biomolecules.

Approximately 150 μg of the $(PLA/HSA)_3$ nanotubes is harvested regularly using a 400 nm porous PC membrane (25 mm ϕ), in which *ca.* 3.0×10^8 effective channels exist. We dispersed the obtained white powder in acidic water (pH 3.5) to dissolve the LbL assembly structure and determined the HSA concentration in

the solution by measuring the absorbance at 280 nm. On the basis of these results, it became apparent that one nanotube (*ca.* 9 μm length) contains *ca.* 2.1×10^6 molecules of HSA.

Wall Thickness of Nanotubes in a Dried State. The $(PLA/HSA)_3$ nanotubes were prepared reproducibly using the PC templates with different pore diameters (D_p = 200, 400, and 800 nm) (Supporting Information Figure S1). The wall thickness was 48−53 nm, independent of the D_p value at the three-cycle depositions (Supporting Information Table S1). We proposed a six-layered cylinder model, in which each HSA layer has single-protein thickness. This model is based on the general principle of LbL membrane growth. The negatively charged HSA binds to the positively charged surface of the PLA layer *via* electrostatic attraction and reverses the surface charge to negative. The monomolecular protein layer turns over the net charge.[20] Subsequently, the next PLA solution makes a new cationic surface on the HSA layer. The average thickness of a PLA/HSA bilayer in our nanotubes is estimated as 16.7 nm. If we assume the dimensions of HSA to be 8 nm from the data of the single-crystal structure[26−28] and small-angle X-ray scattering analyses,[29] then the PLA layer thickness is 8.7 nm. In general, multilayers prepared using LbL assembly within the nanoporous template are thicker than those of corresponding thin films fabricated on a planar substrate with the same number of deposition cycles. Cohen *et al.* created $(PAH/PSS)_{24.5}$ nanotubes [PAH: poly(allylamine hydrochloride)] in the porous PC membrane using a simple immersion and drying technique.[15] The wall thickness was 250 nm (*ca.* 10 nm/bilayer), compared to 155 nm on a flat Si wafer (*ca.* 6 nm/bilayer). Li *et al.* synthesized $(PAH/PSS)_3$ nanotubes in the porous Al_2O_3 membrane using pressure injection.[12] The wall thickness was 50−80 nm (16.7−26.7 nm/bilayer), significantly greater than observed in a smooth configuration.[30] Furthermore, Jonas *et al.* reported an unexpectedly large thickness of the first bilayer (50−120 nm) of poly(vinylbenzyl ammonium chloride) and PSS, which was prepared using vacuum filtration.[17] It was 1−2 orders of magnitude thicker than that of corresponding flat bilayer on a Si wafer (1−3 nm). In view of these investigations, we reasoned that the mode of LbL growth of multilayers in the channel under a certain degree of pressure differs from what occurs during the simple immersion−drying cycle deposition into a pore: the former technique increased the tubes' wall thickness. Several key factors, such as molecular weight and concentration of polymers, ionic strength and pH of the solutions, force of pressure, flow rate, and drying time during the cycle are likely to govern the thickness of the tube wall. The formation details of the polyelectrolyte and protein layers in the porous PC membrane remain unclear in some respects. However, the PLA layer thickness (8.7 nm) in our nanotube is between the reported values for general polyelectrolyte layers prepared in the porous template under pressure conditions.[12,17]

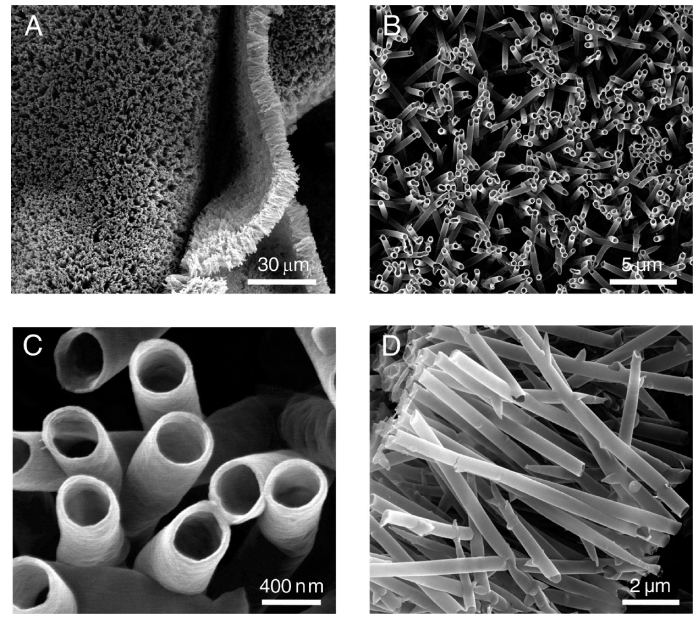

Figure 1. SEM images of $(PLA/HSA)_3$ nanotubes prepared using a 400 nm porous PC template. The lyophilized powders comprise numerous arrays of highly oriented nanotubes.

Normally, for two-cycle filtrations, $(PLA/HSA)_2$ was insufficient to obtain firm nanotubes. For large pores (D_p = 800 nm), the $(PLA/HSA)_3$ cylinders were somewhat fragile, but the six-cycle filtrations (12 layers) provided stiffer nanotubes (Supporting Information Figure S1).

Structures of Protein Nanotubes in Water. The lyophilized $(PLA/HSA)_3$ nanotube powder (*ca.* 50 μg) was suspended in sodium phosphate buffered (PB) solution (10 mM, pH 7.0, 1.5 mL) or deionized water, yielding a homogeneous and slightly turbid dispersion. The SEM images of the evaporated sample on the silicon wafer showed only collapsed aggregates. Our protein nanotubes were unable to endure on the hydrophobic solid surface. To observe the morphology and stability of the $(PLA/HSA)_3$ nanotubes in water, the aqueous dispersions were freeze-dried *in vacuo* at 2, 12, and 24 h after their preparation. Subsequent SEM measurements of the resultant powder revealed that all tubules swelled considerably. Their wall thickness doubled (104 ± 5 nm after 2 h, 106 ± 5 nm after 12 h, and 111 ± 6 nm after 24 h) compared to that of the dried form (Figure 2A,B). It is noteworthy that the direction of the swelling was toward the inside of the hollow and that the outer diameter was unaltered. As a result, a drastic reduction of the inner diameter was found (307 nm → 202 nm after 12 h). This structure is likely to be identical to the fully swollen $(PLA/HSA)_3$ after the LbL growth in the template. To confirm this, we performed SEM measurements of the freeze-dried $(PLA/HSA)_3$ nanotubes embedded within the PC membrane channels. Under these conditions, the wall thickness was *ca.* 100 nm (Figure 2C), the same as that of the isolated nanotube in

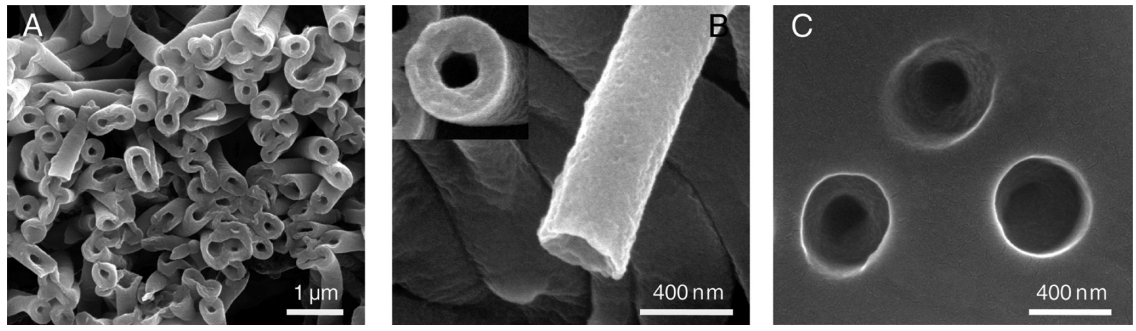

Figure 2. (A,B) SEM images of the lyophilized sample of aqueous dispersion of $(PLA/HSA)_3$ nanotubes (12 h after preparation). (C) SEM images of lyophilized $(PLA/HSA)_3$ nanotubes embedded in PC template (D_p = 400 nm).

aqueous media. We presumed that slow evaporation of water from the wet tubes occurs in the template channel and that a certain degree of shrinkage of the multiple layers takes place in keeping the outer diameter constant. In this dried wall, a gradient of the molecular density might form. Consequently, the liberated protein nanotubes spontaneously returned to their swollen structure by water uptake (*ca.* 400 nm outer diameter, *ca.* 100 nm wall thickness). These morphologies were stable for 24 h; some tubes deformed gradually after 72 h.

The average thickness of a bilayer of PLA/HSA is estimated as 33 nm in a swollen state. Under the assumption that the dimensions of HSA do not change markedly (≤8 nm),[26−29] the PLA layer thickness might be 25 nm, which is apparently large but still similar to that of the polyelectrolyte layers in the tubes prepared under pressure. We estimate the swelling ratio of the PLA layer (α_{PLA}) defined as a ratio between the section area in swollen state and that in dried state. The swelling ratio of PLA is

$$\alpha_{PLA} = \sum_{k=1}^{3} [\pi\{(D_s - (k-1)T_{PLA_s} - (k-1)T_{HSA})^2 - (D_s - kT_{PLA_s} - (k-1)T_{HSA})^2\}/4]/ \sum_{k=1}^{3} [\pi\{(D_d - (k-1)T_{PLA_d} - (k-1)T_{HSA})^2 - (D_s - kT_{PLA_d} - (k-1)T_{HSA})^2\}/4] \quad (1)$$

where D_s and D_d, respectively, represent the outer diameters of the nanotubes in swollen and dried states, T_{HSA} is the thickness of the HSA layer,[26−29] and T_{PLA_s} and T_{PLA_d}, respectively, represent thicknesses of the PLA layers in swollen and dried states. The α_{PLA} was calculated as 2.5, which is similar to published values for general synthetic polyelectrolytes (1.2−4.0).[31,32]

The biological function of HSA in the tube will only be retained if the protein structure is preserved. In our earlier work, we fabricated a LbL thin film of $(PEI/HSA)_n$ (PEI: polyethyleneimine) on the flat quartz plate and reported that the CD spectral pattern and intensity of the HSA layer increased in proportion to the layer number.[23] Those results imply that the secondary structure of HSA is unaffected by complexation with PLA. Here we employed FT-IR spectroscopy to characterize the protein amide I band at 1650−1660 cm^{-1} (mainly attributed to C═O stretching vibrations) and amide II band at 1540−1560 cm^{-1} (C−N stretching coupled with N−H bending vibrations). Both are sensitive markers of the change of the protein secondary structure.[33,34] Since the polypeptide backbone of PLA also contributes to the IR spectrum, we prepared $(PEI/HSA)_3$ nanotubes using high molecular weight PEI (M_w = 70 000) following the same synthetic protocol. The tubes prepared in this manner were dispersed in water and again freeze-dried. The amide I and II bands of free HSA appeared at 1656 and 1545 cm^{-1}, respectively (Supporting Information Figure S2), and are quite similar to the values reported elsewhere.[33,34] The $(PEI/HSA)_3$ nanotubes also demonstrated two intense amide I and II bands at completely the same positions as free HSA. Our FT-IR studies show no marked difference in the protein secondary structure between the free HSA and HSA components in the nanotubes.

Molecular Capture by the Cylindrical Walls. HSA is the most prominent plasma protein in the human circulatory system and acts as a transporter or depot of insoluble endogenous and exogenous compounds, such as fatty acids, hemin, bilirubin, thyroxine, metal ions, and a broad range of drugs.[35,36] If the HSA components in the $(PLA/HSA)_3$ nanotubes retain their original ligand binding ability, the tubules are also able to bind the molecules.

Uranyl ion (UO_2^{2+}), a widely used negative staining agent for TEM, binds strongly to the subdomain IIB of HSA.[37] TEM observations of lightly stained $(PLA/HSA)_3$ nanotubes using 0.05% uranyl acetate yielded positive images of the cylindrical hollows (Figure 3A), indicating that the UO_2^{2+} binds to the protein nanotubes. Remarkably, the inner wall of the cylinder was somewhat dark, perhaps because the sixth and most accessible layer of the nanotube was constituted of HSA. Use of 0.25% uranyl acetate yielded a much darker image, in which the nanotubular wall was fully stained (Figure 3B). Nevertheless, it is still evident that the inner wall of the hollow was more strongly stained than the outer PLA layer. In contrast, staining by 0.5% (1-thio-D-glucopyranosato)gold (Glu-Au) elicited negative im-

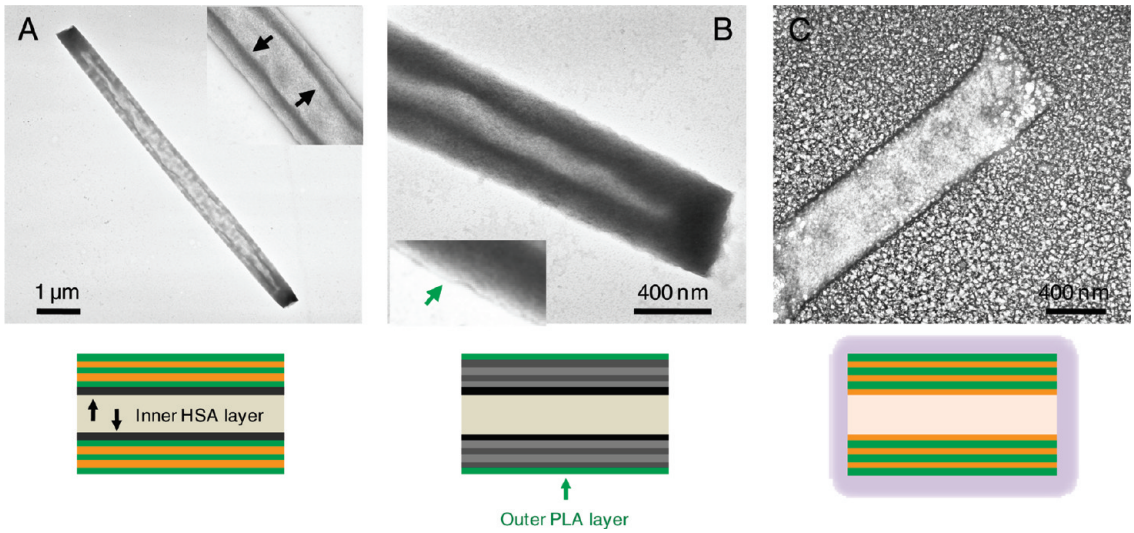

Figure 3. TEM images of $(PLA/HSA)_3$ nanotubes stained with (A) 0.05% $UO_2(AcO)_2$, (B) 0.25% $UO_2(AcO)_2$, and (C) 0.5% Glu-Au.

ages because Glu-Au cannot penetrate the multilayered 100 nm thick walls (Figure 3C). All of these results show that the $(PLA/HSA)_3$ nanotubes capture the UO_2^{2+} ions into their HSA layers.

Next, we exploited 3,3′-diethylthiacarbocyanine iodide (DTC), which is a positively charged fluorescent ligand for HSA with a binding constant (K) of 1.1×10^4 M^{-1}.[38] The DTC was added to the PB solution (pH 7.0, 10 mM) of the $(PLA/HSA)_3$ nanotubes ([DTC] = 0.2 μM). Then the mixture was incubated for 3 h in the dark at room temperature. The resultant dispersion was centrifuged for 10 min at 4000g to remove the tubes. The fluorescence intensity of the supernatant was significantly lower (36%) than that of the identically treated DTC solution without the tubes (Figure 4A(i))). Incubation with the $(PLA/PLG)_3$ nanotubes, in which poly-L-glutamic acid sodium salt (PLG) was used instead of HSA, did not decrease the fluorescence intensity of the DTC solution. This implies that the HSA layer is required to capture the DTC, and a nonspecific adhesion of the ligand onto the outer surface of the tube is excluded. Here two binding modes are feasible: (i) DTC is bound only to the inner surface layer (sixth layer) of HSA or (ii) DTC can diffuse into the swollen wall and is bound to the all HSA layers. To clarify this point, we fabricated $(PLA/HSA)_3PLA$ nanotubes, in which the internal surface of HSA was blocked by an additional PLA layer. The fluorescence of DTC solution with the $(PLA/HSA)_3PLA$ nanotubes declined to 36% of the control, which is precisely the same result as that of the $(PLA/HSA)_3$ nanotubes (Figure 4A(i)). On the basis of these results, it can be concluded that the rapid diffusion of DTC through the tubular wall occurs and the ligand is bound to the HSA components (Figure 4B). The ratio of the DTC/HSA was estimated as *ca.* 0.6/1 (mol/mol).

Rhodamine 123 (R123) is a positively charged fluorescent dye that is often used to monitor the membrane potential of mitochondria but is *not* a ligand for HSA.[39] The same fluorescence measurements showed that neither $(PLA/HSA)_3$ nor $(PLA/HSA)_3PLA$ nanotubes interacted with R123 (Figure 4A(ii),B), consistent with our expectation.

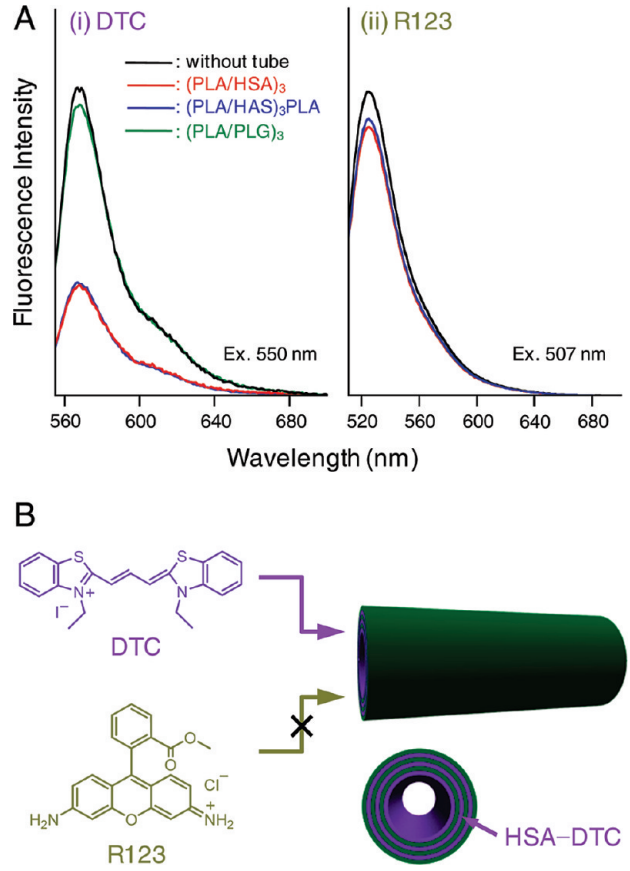

Figure 4. (A) Fluorescence spectra of the PB solution (pH 7.0, 10 mM) of (i) DTC (0.2 μM) and (ii) R123 (0.2 μM) after incubation with protein nanotubes, with subsequent centrifugation (4000g, 10 min). (B) Schematic illustration of ligand capture in $(PLA/HSA)_3$ nanotubes. The DTC diffuses in the cylindrical wall and is bound to the HSA layers of the tubes.

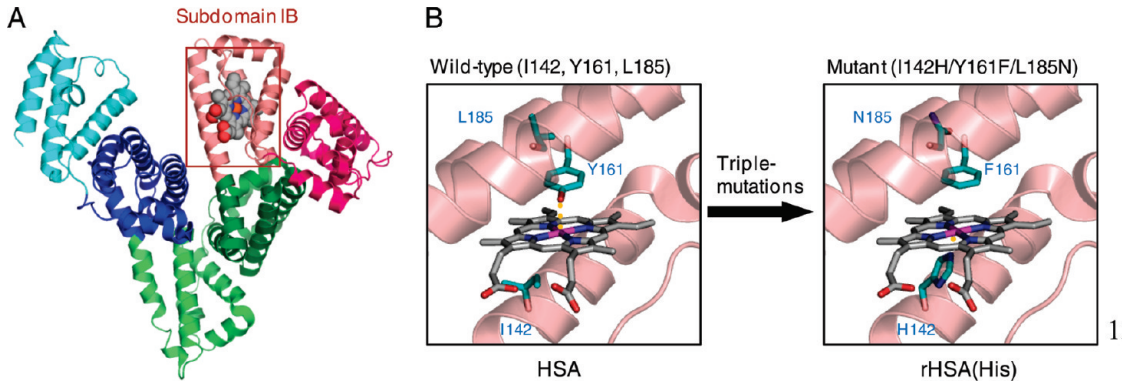

Figure 5. (A) Crystal structure of HSA−FePP complex (code: 1O9X[42]).[43] Here, FePP is shown in a space-filling representation. (B) Structural models of HSA complexed with FePP or ZnPP in subdomain IB. In HSA (wild-type), Tyr-161 axially coordinates to the central metal ion of porphyrin. In rHSA(His), His-142 coordinates to the central metal of porphyrin from the opposite side of the ring plane.

It is known that hemin [iron(III) protoporphyrin IX, FePP] dissociated from methemoglobin is captured by HSA in the human circulatory system and then transported to the liver for catabolism.[40] Crystallographic studies of the HSA−FePP complex revealed that the FePP was bound within a D-shaped hydrophobic cavity in subdomain IB of HSA (Figure 5A).[41,42] The central iron atom is weakly coordinated by phenolate oxygen of Tyr-161 (Figure 5B). We found that zinc(II) protoporphyrin IX (ZnPP) is also accommodated into the same pocket with a binding constant of 4.4×10^5 M^{-1}, and that the HSA−ZnPP complex acts as a photosensitizer for hydrogen generation from water.[44] The fluorescence intensity of the ZnPP solution incubated with the $(PLA/HSA)_3$ nanotubes decreased to 13% relative to that of the identically treated ZnPP solution without the tubes (Figure 6A(i)). The following results strongly suggest that the ZnPP diffuses in the tube walls and mainly binds to the three layers of HSA: the fluorescence intensity of the ZnPP solution mixed with the $(PLA/HSA)_3PLA$ nanotubes declined to 10% of the control value (Figure 6A(i)), whereas 82% fluorescence remained after incubation with the $(PLA/PLG)_3$ nanotubes (data not shown). The ratio of ZnPP/HSA was estimated as *ca.* 0.7/1 (mol/mol).

Using site-directed mutagenesis, we can confer an O_2 binding capability on the HSA−FePP complex.[45,46] In particular, triple mutations in subdomain IB, (i) introduction of His into the Ile-142 position, (ii) replacement of the coordinated Tyr-161 by the hydrophobic Phe, and (iii) insertion of Asn into the Leu-185 position as a distal base created an artificial heme pocket involving a axial His-142 ligation to the prosthetic FePP group (Figure 5B).[45,46] The reduced form of the recombinant HSA mutant [rHSA(His)]−Fe(II)PP complex reversibly binds O_2 in much the same way as hemoglobin. The ZnPP is also bound into this genetically engineered heme pocket of rHSA(His).[44] The binding constant (K) of ZnPP for rHSA(His) in 15% DMSO/PB solution was determined as 1.4×10^6 M^{-1}, which is three times higher than that found for HSA (4.4×10^5 M^{-1}). The axial coordination of the imidazolyl group of His-142 to the central zinc(II) ion of ZnPP appears to enhance the binding affinity to the protein. Then we prepared new nanotubes using rHSA(His) instead of HSA: $(PLA/rHSA(His))_3$ nanotubes. The TEM images of the dried sample showed formation

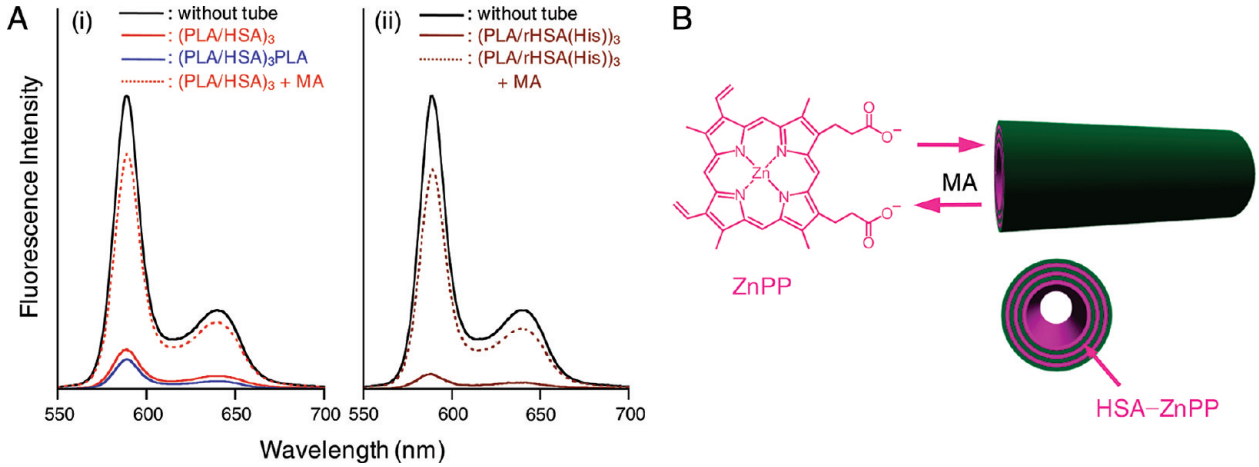

Figure 6. (A) Fluorescence spectra of 15% DMSO/PB solution (pH 7.0, 10 mM) of ZnPP (0.2 μM) after incubation with (i) $(PLA/HSA)_3$ nanotubes or (ii) $(PLA/rHSA(His))_3$ nanotubes, with subsequent centrifugation (4000*g*, 10 min). (B) Schematic illustration of ZnPP capture in $(PLA/HSA)_3$ nanotubes. Addition of MA caused release of the loaded ZnPP.

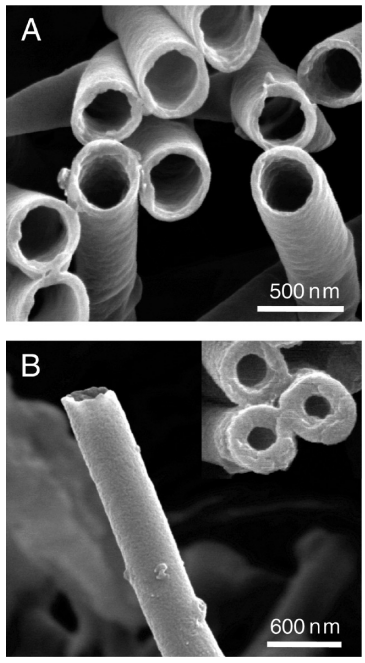

Figure 7. SEM images of (A) $(PLA/HSA)_2PLA/PLG/Avi$ nanotubes prepared using a 400 nm porous PC template and (B) lyophilized sample of their aqueous dispersion.

of similar cylinders with 412 ± 11 nm outer diameter (Supporting Information Figure S3). As expected, these nanotubes captured ZnPP more effectively than nanotubes prepared with wild-type HSA. The free concentration of ZnPP was reduced to 5% (Figure 6A(ii)), and the binding ratio of ZnPP/HSA increased to *ca.* 0.8/1 (mol/mol). The resuspended solution of the ZnPP-loaded $(PLA/rHSA(His))_3$ nanotubes showed fluorescence maxima at 596 and 649 nm, indicating the axial His coordination to ZnPP in the protein components.[44] The combined structural and mutagenic approaches enable us to enhance the molecular capturing properties of the HSA nanotubes.

For practical applications, such as drug delivery and molecular separation, the bound ligands should be released from the nanotubes.[6,16] Rubner *et al.* reported drug release from the $(PAH/PSS)_n$ nanotubes by drastically changing the solution pH.[16] Here we exploited a ligand replacement reaction of HSA to dissociate the captured molecule at pH 7.0. Fatty acids are a typical ligand for HSA.[35,36] On the basis of systematic crystal structure analyses, Curry *et al.* revealed seven binding sites for fatty acids ($C_{10}-C_{22}$) in HSA (FA sites 1−7).[27,28] One of them (FA site 1) is a common site with FePP, which is a heme pocket in subdomain IB[42] (Supporting Information Figure S4), suggesting that the bound ZnPP would be released by addition of excess moles of fatty acid. As expected, addition of MA to the ZnPP-loaded $(PLA/HSA)_3$ nanotubes ([MA] = 1 mM) caused a marked increase of the fluorescence intensity up to 80% of the control value within 10 min (Figure 6A(i)). This rapid release of ZnPP from the nanotubes can be attributed to

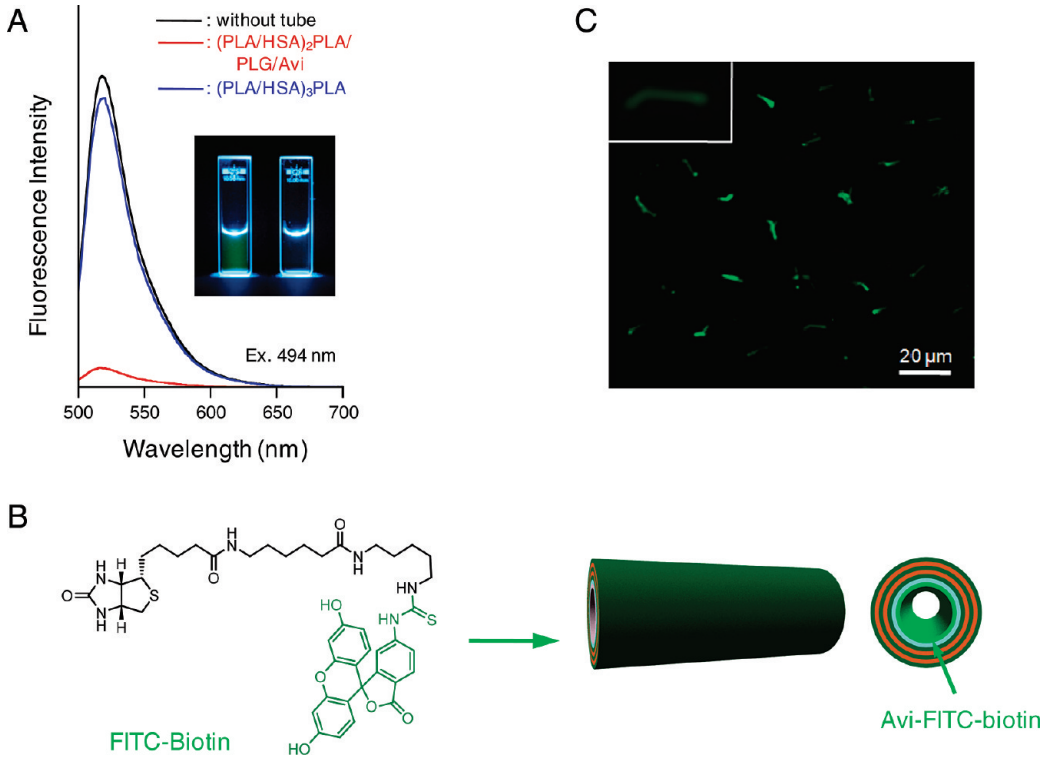

Figure 8. (A) Fluorescence spectra of PB solution (pH 7.0, 10 mM) of FITC-biotin (0.2 μM) after incubation with $(PLA/HSA)_2PLA/PLG/Avi$ nanotubes, with subsequent centrifugation (4000*g*, 10 min). (Inset) Photograph of (left) PB solution of FITC-biotin (0.2 μM) and (right) supernatant treated with $(PLA/HSA)_2PLA/PLG/Avi$ nanotubes. (B) Schematic illustration of FITC-biotin capture in $(PLA/HSA)_2PLA/PLG/Avi$ nanotubes. (C) CLSM image of FITC-biotin capture in $(PLA/HSA)_2PLA/PLG/Avi$ nanotubes (ex. at 488 nm).

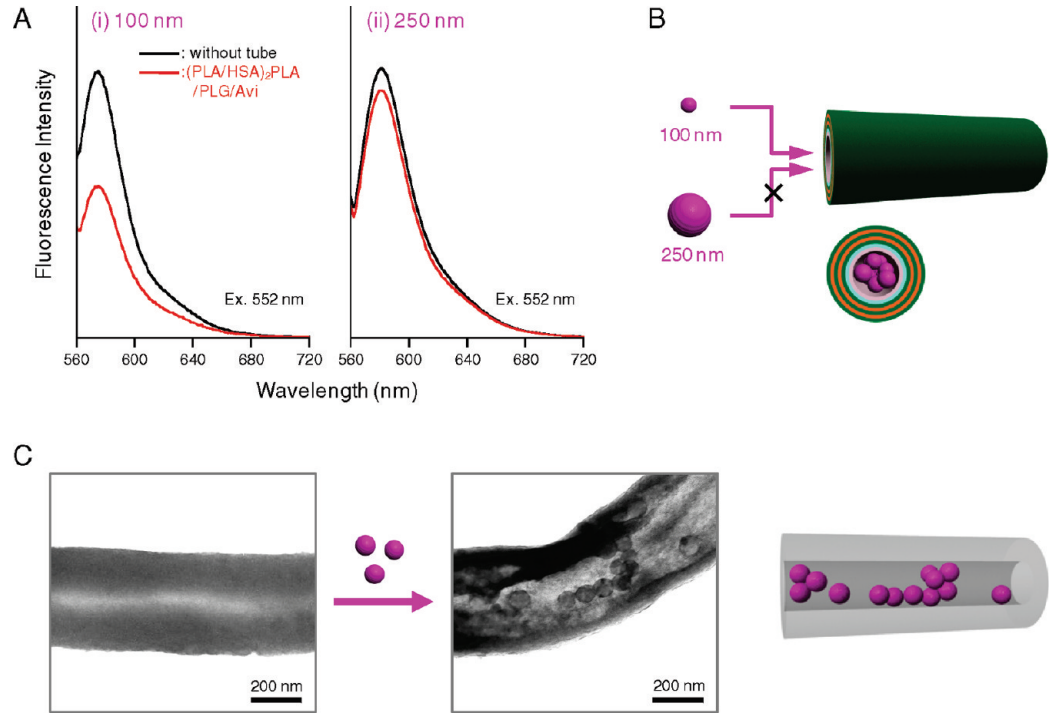

Figure 9. (A) Fluorescence spectra of supernatant of PB solution (pH 7.0, 10 mM) of (i) 100 nm biotin-FNPs (5.0×10^{10} particles/mL) and (ii) 250 nm biotin-FNPs (7.7×10^{9} particles/mL) after incubation with $(PLA/HSA)_2PLA/PLG/Avi$ nanotubes, with subsequent centrifugation (4000*g*, 10 min). (B) Schematic illustration of biotin-FNP capture in $(PLA/HSA)_2PLA/PLG/Avi$ nanotubes. (C) TEM images of $(PLA/HSA)_2PLA/PLG/Avi$ nanotubes before and after incorporation of 100 nm biotin-FNPs.

the replacement of ZnPP by MA in the HSA component. The remaining ZnPP (20%), which is probably located in the PLA layer, did not emerge upon addition of MA. For $(PLA/rHSA(His))_3$ nanotubes, the fluorescence increased to 75% of the control value by addition of MA (Figure 6B(ii)). The slightly lower release ratio could be due to the strong binding affinity of ZnPP for rHSA(His).

Molecular Capture in Cylindrical Pores. To promote the biospecific capturing capability of the protein nanotubes further, we introduced avidin (Avi, $M_w = 68\,000$) as the last layer of the tube wall. The Avi from egg white binds four biotins with the highest affinity of any known protein ($K > 10^{15}$ M^{-1}).[47] We prepared $(PLA/HSA)_2PLA/PLG/Avi$ nanotubes using the same procedure. Because Avi is a basic glycoprotein (isoelectric point = 10.0−10.5) and has positive net charges at pH 7.0, the fifth PLA layer was covered by an anionic PLG before Avi layer fixation. The SEM images taken of the lyophilized sample showed the formation of uniform cylinders with an outer diameter of 403 ± 10 nm and a wall thickness of 59 ± 5 nm (Figure 7A). Under aqueous conditions, the multilayered walls swelled significantly by water uptake in a similar fashion to that of the $(PLA/HSA)_3$ nanotubes (Figure 7B) (416 ± 11 nm outer diameter, 130 ± 9 nm wall thickness).

As a ligand for this hybrid protein nanotube, we exploited 5-(6′-biotinamidohexanoylamino)-pentylthioureidylfluorescein (FITC-biotin), which has a long flexible spacer chain between the biotin and fluorescein moieties. The fluorescence intensity of the PB solution (10 mM, pH 7.0) of FITC-biotin disappeared after incubation with the $(PLA/HSA)_2PLA/PLG/Avi$ nanotubes (Figure 8A). Bleaching of the color was clearly apparent (Figure 8A, inset), while supernatant treated with the $(PLA/HSA)_3PLA$ nanotubes fluoresced as strongly as the control solution, signifying that FITC-biotin was bound to the single wall of the Avi layer (Figure 8B). The binding ratio of the FITC-biotin and Avi was estimated to be *ca.* 3.4/1 (mol/mol). The FITC-biotin-loaded $(PLA/HSA)_2PLA/PLG/Avi$ nanotubes, which were collected by centrifugation, fluoresced strongly, as revealed by CLSM measurements (ex. at 488 nm) (Figure 8C). Similar $(PLA/HSA)_3Avi$ nanotubes could be also prepared, but they did not capture FITC-biotin efficiently. The last avidin layer was probably not deposited well on the HSA layer.

Finally, we attempted to capture fluorescent nanoparticles (FNPs) in the one-dimensional space interior of the $(PLA/HSA)_2PLA/PLG/Avi$ nanotubes. Fluorescent latex beads bearing NH_2 groups on the surface (100 or 250 nm)[48] were reacted with sulfosuccinimidyl-6-(6′-biotinamidohexanoylamino)hexanoate, yielding biotinylated FNPs (biotin-FNPs). The degree of the biotinylation of the NH_2 groups was determined using HABA assay:[49] 48% for the 100 nm particles and 50% for the 250 nm particles.

The fluorescence intensity of the PB (10 mM, pH 7.0) solution of 100 nm biotin-FNPs (5.0×10^{10} particles/mL) was diminished after incubation with the $(PLA/HSA)_2PLA/PLG/Avi$ nanotubes (Figure 9A(i)), which

suggests that the nanoparticles were incorporated into the hollows (Figure 9B). In contrast, the decrease in fluorescence was negligible after incubation with 250 nm biotin-FNPs (7.7×10^9 particles/mL) (Figure 9A(ii)). This difference showed that the larger biotin-FNPs cannot enter the tube because the nanotube pores (*ca.* 200 nm) are smaller than the particle diameter (Figure 9B). Careful inspection of the fluorescence spectrum revealed that the average quantities of the 100 nm biotin-FNPs captured into the pore were calculated as 161 per tube. This means that the occupancy ratio of the particles in volume was 29%. The obtained TEM images of the nanotubes collected by centrifugation showed a line of the entrapped biotin-FNPs in the cylindrical pore (Figure 9C). The filling ratio of the particles in the hollow from the TEM picture was 23%, which is broadly equivalent to the value from the fluorescence measurements. The red fluorescent nanotubes observed in CLSM also supported the loading of 100 nm biotin-FNPs into the tube (Supporting Information Figure S5).

CONCLUSIONS

We have shown that supramolecular templating synthesis using nanoporous PC membrane combined with dissolution of the template with DMF and freeze-drying of the extracted cores can be used to prepare robust protein nanotubes. Notably, the powder obtained from this procedure consisted of a thin layer sheet of the uniform arrays of the tubes. The protein nanotubes swelled considerably under aqueous conditions. We can confer molecular capturing capabilities on both the cylindrical wall and one-dimensional space interior using ligand−protein interactions. UO_2^{2+}, DTC, and ZnPP are able to diffuse into the multilayered walls of the tubules, where they are captured by HSA components. Introduction of histidine into the subdomain IB of HSA by site-specific mutations enhanced the binding constant of ZnPP. As a result, the recombinant HSA-based nanotubes can capture numerous ligands. Furthermore, the bound ZnPPs are released to the bulk aqueous solution by ligand replacement with MA because they bind competitively to the same position in subdomain IB of HSA. The introduction of Avi layers as an internal pore surface enables the nanotubes to entrap biotin derivatives tightly. Biotin-labeled FNPs were also incorporated into the pores when their particle size is smaller than the tube's inner diameter. This suggests that simply depositing a specific protein at the last layer of the cylinders would enable us to create desired loading and release systems to be used as separation devices in biomedical fields. In some instances, nanotubes having an antibody inner wall might conceivably be exploited as a size-selective trap for infectious viruses. The flexibility of molecular architecture of the protein nanotubes is stimulating efforts to develop an enzymatic chemical reactor.

EXPERIMENTAL SECTION

Materials and Apparatus. Poly-L-arginine hydrochloride (PLA, M_w = *ca.* 70 000), poly-L-glutamic acid sodium salt (PLG, M_w = 50 000−100 000), human serum albumin (HSA, recombinant product expressed by yeast species *Pichia pastoris*), rhodamine 123 hydrate (R123), 3,3′-diethylthiacarbocyanine iodide (DTC), zinc(II) protoporphyrin IX (ZnPP), and 5-(6′-biotinamidohexanoylamino)pentylthioureidylfluorescein (FITC-biotin) were purchased from Sigma-Aldrich Co. Avidin from egg white (Avi), myristic acid (MA), and (1-thio-D-glucopyranosato)gold (Glu-Au) were purchased from Wako Pure Chemical Industries, Ltd. Polyethylenimine branched (PEI, M_w = 70 000) was purchased from Alfa Aesar. The water was deionized (18.2 MΩcm) using water purification systems (Elix UV and Simpli Lab-UV; Millipore Corp.). The preparation protocol of recombinant human serum albumin I142H/Y161F/L185N mutant [rHSA(His)] was as described previously.[46] The UV−vis absorption spectra were obtained using a UV−visible spectrophotometer (8453; Agilent Technologies, Inc.) equipped with a temperature control unit (89090A; Agilent). Fluorescence emission spectra were measured using a spectrofluorometer (FP-6500; Jasco Inc.).

Template Synthesis of Protein Nanotubes. The protein nanotubes were prepared according to our previously reported techniques with several modifications. Typically, the $(PLA/HSA)_3$ nanotubes were prepared as follows. The track-etched polycarbonate (PC) membrane (Isopore membrane, 25 mm ϕ, pore diameter (D_p) 200, 400, or 800 nm; Millipore Corp.) was placed into a stainless steel syringe holder (25 mm; Advantec Mfs, Inc.). The sodium phosphate buffer (PB) solution (pH 7.0, 10 mM, 10 mL) of PLA (1 mg/mL) containing 0.1 M NaCl was first filtered through the membrane (0.25 mL/min) using a syringe pump (PHD-2000; Harvard Apparatus). The positively charged PLA absorbed onto the negatively charged pore surfaces of the PC template. Then excess PLA was washed by the filtration of deionized water (10 mL, 1.0 mL/min); the membrane was dried *in vacuo* for 10 min. Next, the PB solution (pH 7.0, 10 mM, 10 mL) of HSA (2 mg/mL) was injected (0.5 mL/min) to generate the second layer of negatively charged HSA on the PLA surface. After washing with water (10 mL, 1.0 mL/min) to remove loosely adsorbed protein, the membrane was dried again under vacuum for 10 min. These pressure infiltrations using the syringe pump were repeated for three cycles. The oppositely charged PLA and HSA alternately deposit onto the PC membrane's pore wall to grow the LbL thin film of PLA/HSA. The PC membrane was then removed from the holder, wiped gently using a cotton swab with water to eliminate adherent layers that were present on the top and bottom surfaces, and dried in an automatic low-humidity chamber (Super Dry; Toyo Living Co. Ltd., Japan) for 12 h (humidity ≤1%). To release the protein nanotubes from the PC template, the membrane was immersed into a DMF solution at room temperature. The porous PC was dissolved immediately, and the liberated nanotubes were precipitated. The supernatant was discarded carefully, and the remaining nanotubes were washed twice with DMF. Finally, the dispersion was freeze-dried *in vacuo* (below 20 Pa), yielding the lyophilized $(PLA/HSA)_3$ nanotubes as many small pieces of thin film. Although tetrahydrofuran (THF) is also applicable for dissolving the PC template, DMF yields good tubular alignment.

Other protein nanotubes [$(PLA/rHSA(His))_3$, $(PLA/HSA)_2PLA/PLG/Avi$), and $(PEI/HSA)_3$] were also fabricated using the same procedure. The PB solution (pH 7.0, 10 mM, 10 mL) of PLG (1.0 mg/mL), rHSA(His) (2.0 mg/mL), and Avi (1.0 mg/mL) and the PB solution (pH 7.0, 10 mM, 10 mL) of PEI (1.0 mg/mL) containing 0.1 M NaCl were used for the preparations.

Scanning Electron Microscopy (SEM) and Transmission Electron Microscopy (TEM) Observations. For SEM measurements of the nanotubes, the lyophilized sample was fixed directly on the carbon

tape and sputter-coated with Pd−Pt using an ion sputter (E-1045; Hitachi Ltd.). The SEM observations were performed using a scanning electron microscope (S-4300; Hitachi Ltd.) with an accelerating voltage of 10 kV. To fix the swollen morphologies of the nanotubes in water, the aqueous dispersion in the cryotube was plunged into a liquid nitrogen bath and freeze-dried under a vacuum. For each sample, at least 50 different nanotubes were measured to obtain an average size of the outer diameter and wall thickness.

For TEM observations, 3 μL of the aqueous solution of the nanotubes was placed onto an elastic carbon-coated copper grid (100 mesh; Okenshoji Co. Ltd.), which was hydrophilized using a hydrophilic treatment device (HDT-400; JEOL Datum). The air-dried samples were then stained with 3 μL of aqueous uranyl acetate or aqueous Glu-Au. After 1 min, the excess fluid was removed using filter paper and the grids were again air-dried at room temperature. These specimens were observed using a transmission electron microscope (JEM-1011; JEOL) with an accelerating voltage of 100 kV.

FT-IR Measurements of Protein Nanotubes. The FT-IR spectra of the KBr disk containing lyophilized powder of free HSA or $(PEI/HSA)_3$ nanotubes were measured using an FT-IR spectrophotometer (FT/IR-4200; Jasco Inc.). The spectra at 4 cm^{-1} resolution were accumulated 64 times to improve the signal-to-noise ratio.

Preparation of Biotin-Labeled Fluorescent Nanoparticles (Biotin-FNPs). Fluorescent latex nanoparticles bearing NH_2 groups on the surface (100 and 250 nm diameter, Micromer-redF) were purchased from Micromod Partikeltechnologie GmbH. The phosphate buffered saline (PBS) solution (pH 7.4, 25 μL) of sulfosuccinimidyl-6-(6′-biotinamidohexanoylamino)hexanoate (Pierce Biotechnology, Inc.) (10 mg/mL) was added to the PBS solution of Micromer-redF (100 nm) (9.1 mg/mL, 0.55 mL) (biotin/NH_2 group: 0.5/1). Then the mixture was stirred for 30 min in the dark at room temperature. The nanoparticles were then washed with PBS solution using centrifugal filter devices (Ultracel Y30; Amicon Inc.) and concentrated to the initial volume. The 250 nm particles were also biotinylated similarly. The biotin-labeled ratio of the surface NH_2 groups of the nanoparticles was assayed using Green's procedure with 2-(4′-hydroxybenzenazo)benzoic acid (HABA; Fluka Chemika GmbH).[49]

Molecular Capture in Protein Nanotubes. The lyophilized powder of the protein nanotubes (*ca.* 50 μg) was dispersed in the PB solution (pH 7.0, 10 mM, 1.5 mL). Then the mixture was sonicated for a few seconds and transferred to a 10 mm path length optical quartz cuvette. Ligand stock solutions were prepared in water (R123), *N*-methyl pyrrolidone (DTC and FITC-biotin), DMSO (ZnPP), or PBS (biotin-FNPs). Several microliters of the ligand solutions (<1% of the total volume) were added to the nanotube dispersions to achieve a typical concentration of 0.2 μM. For ZnPP, the nanotubes were dispersed into 15% DMSO/PB solution because of the low solubility of ZnPP. The dispersion was transferred to a glass tube and centrifuged for 10 min at 4000*g* to collect the nanotubes. The fluorescence of the supernatant was measured to assay the concentration of the noncaptured free ligand in the bulk solution. An identically treated control sample without nanotubes was always prepared simultaneously; its fluorescence intensity was regarded as a 100% ligand concentration. To release the bound ZnPP from the nanotubes, the DMSO solution of MA was added (less than 2% of the whole volume) and heated briefly when MA was not sufficiently dissolved.

Determination of Binding Constant of ZnPP for HSA and rHSA(His). Binding constants (*K*) of ZnPP for HSA and rHSA(His) were determined using fluorescence quenching measurements of albumin by ZnPP titration according to the literature.[50] The fluorescence of the HSA or rHSA(His) (2.5 μM) (ex. 280 nm) in PB solution (pH 7.0, 10 mM) including 15% DMSO was quenched upon binding of ZnPP. The data were treated using the double-log method [$\log(F_o - F)/(F_o - F_\infty)$ *vs* $\log$[ZnPP], where F_o is the original fluorescence of the protein, F is the observed fluorescence in the presence of a given amount of ZnPP, and F_∞ is the fluorescence of fully formed complex] to obtain the *K* values.

Confocal Laser Scanning Microscopy (CLSM) Observations. CLSM measurements were performed using a laser scanning microscope (LSM 510; Carl Zeiss Inc.). A droplet of the aqueous solution of the $(PLA/HSA)_2PLA/PLG/Avi$ nanotubes incorporating FITC-biotin or biotin-FNP was air-dried on the cover glass and applied directly to the observations (ex. 488 nm).

Acknowledgment. This work was supported by PRESTO "Control of Structure and Functions" JST, Grant-in-Aid for Scientific Research for Priority Area "Coordination Programming" (area 2107) from MEXT Japan, and Grant-in-Aid for Scientific Research (B) (No. 20350058) from JSPS. Skillful experiments on synthesis of protein nanotubes conducted by Ms. Nao Kobayashi and Ms. Hiromi Terada are gratefully acknowledged. We thank Prof. Dr. Stephen Curry (Imperial College London) for his comments on ligand binding to HSA and critical reading of the manuscript. X.Q. acknowledges a JSPS Postdoctoral Fellowship for Foreign Researchers.

Supporting Information Available: SEM images of $(PLA/HSA)_3$ nanotubes prepared using a 200 nm porous PC template and $(PLA/HSA)_6$ nanotubes prepared using a 800 nm porous PC template (Figure S1), dimensions of $(PLA/HSA)_n$ nanotubes (Table S1), FT-IR spectra of $(PEI/HSA)_3$ nanotubes (Figure S2), TEM image of $(PLA/rHSA(His))_3$ nanotubes prepared using a 400 nm porous PC template (Figure S3), structural model of subdomain IB of HSA showing the comparative binding configurations of ZnPP and MA (Figure S4), and CLSM image of biotin-FNP-loaded $(PLA/HSA)_2PLA/PLG/Avi$ nanotubes (Figure S5). This material is available free of charge *via* the Internet at http://pubs.acs.org.

REFERENCES AND NOTES

1. Martin, C. R. Nanomaterials: A Membrane-Based Synthetic Approach. *Science* **1994**, *266*, 1961–1966.
2. Steinhart, M.; Wehrspohn, R. B.; Gösele, U.; Wendorff, J. H. Nanotubes by Template Wetting: A Modular Assembly System. *Angew. Chem., Int. Ed.* **2004**, *43*, 1334–1344.
3. Steinhart, M. Supramolecular Organization of Polymeric Materials in Nanoporous Hard Templates. *Adv. Polym. Sci.* **2008**, *220*, 123–187.
4. Hou, S.; Harrell, C. C.; Trofin, L.; Kohli, P.; Martin, C. R. Layer-by-Layer Nanotube Template Synthesis. *J. Am. Chem. Soc.* **2004**, *126*, 5674–5675.
5. Hou, S.; Wang, J.; Martin, C. R. Template-Synthesized DNA Nanotubes. *J. Am. Chem. Soc.* **2005**, *127*, 8586–8587.
6. Son, S. J.; Reichel, J.; He, B.; Schuchman, M.; Lee, S. B. Magnetic Nanotubes for Magnetic-Field-Assisted Bioseparation, Biointeraction, and Drug Delivery. *J. Am. Chem. Soc.* **2005**, *127*, 7316–7317.
7. Huang, J.; Kunitake, T. Nanotubings of Titania/Polymer Composite: Template Synthesis and Nanoparticle Inclusion. *J. Mater. Chem.* **2006**, *16*, 4257–4264.
8. Wang, Y.; Angelatos, A. S.; Caruso, F. Template Synthesis of Nanostructured Materials *via* Layer-by-Layer Assembly. *Chem. Mater.* **2008**, *20*, 848–858.
9. Yu, A.; Lu, G. Q. M.; Drennan, J.; Gentle, I. R. Tubular Titania Nanostructures *via* Layer-by-Layer Self-Assembly. *Adv. Funct. Mater.* **2007**, *17*, 2600–2605.
10. He, Q.; Cui, Y.; Ai, S.; Tian, Y.; Li, J. Self-Assembly of Composite Nanotubes and Their Applications. *Curr. Opin. Colloid Interface Sci.* **2009**, *14*, 115–125.
11. Liang, Z.; Sucha, A. S.; Yu, A.; Caruso, F. Nanotubes Prepared by Layer-by-Layer Coating of Porous Membrane Templates. *Adv. Mater.* **2003**, *15*, 1849–1853.
12. Ai, S.; Lu, G.; He, Q.; Li, J. Highly Flexible Polyelectrolyte Nanotubes. *J. Am. Chem. Soc.* **2003**, *125*, 11140–11141.
13. Yang, Y.; He, Q.; Duan, L.; Cui, Y.; Li, J. Assembled Alginate/Chitosan Nanotubes for Biological Application. *Biomaterials* **2007**, *28*, 3083–3090.
14. Kim, D. H.; Karan, P.; Göring, P.; Leclaire, J.; Caminade, A.-M.; Majoral, J.-P.; Gösele, U.; Steinhart, M.; Knoll, W. Formation of Dendrimer Nanotubes by Layer-by-Layer Deposition. *Small* **2005**, *1*, 99–102.
15. Lee, D.; Nolte, A. J.; Kunz, A. L.; Rubner, M. F.; Cohen, R. E. pH-Induced Hysteric Gating of Track-Etched Polycarbonate Membrane: Swelling/Deswelling Behavior of Polyelectrolyte Multilayers in Confined Geometry. *J. Am. Chem. Soc.* **2006**, *128*, 8521–8529.

16. Lee, D.; Cohen, R. E.; Rubner, M. F. Heterostructured Magnetic Nanotubes. *Langmuir* **2007**, *23*, 123–129.
17. Alem, H.; Blondeau, F.; Glinel, K.; Demoustier-Champagne, S.; Jonas, A. M. Layer-by-Layer Assembly of Polyelectrolytes in Nanopores. *Macromolecules* **2007**, *40*, 3366–3372.
18. Hou, S.; Wang, J.; Martin, C. R. Template-Synthesized Protein Nanotubes. *Nano Lett.* **2005**, *5*, 231–234.
19. Hillebrenner, H.; Buyukserin, F.; Stewart, J. D.; Martin, C. R. Bifunctionalization and Capping of Template Synthesized Nanotubes. *J. Nanosci. Nanotechnol.* **2007**, *7*, 2211–2221.
20. Yu, A.; Liang, Z.; Caruso, F. Enzyme Multilayer-Modified Porous Membranes as Biocatalysts. *Chem. Mater.* **2005**, *17*, 171–175.
21. Lu, G.; Ai, S.; Li, J. Layer-by-Layer Assembly of Human Serum Albumin and Phospholipid Nanotubes Based on a Template. *Langmuir* **2005**, *21*, 1679–1682.
22. Tian, Y.; He, Q.; Cui, Y.; Li, J. Fabrication of Protein Nanotubes Based on Layer-by-Layer Assembly. *Biomacomolecules* **2006**, *7*, 2539–2542.
23. Qu, X.; Lu, G.; Tsuchida, E.; Komatsu, T. Protein Nanotubes Comprised of an Alternate Layer-by-Layer Assembly Using a Polycation as an Electrostatic Glue. *Chem.—Eur. J.* **2008**, *14*, 10303–10308.
24. Landoulsi, J.; Roy, C. J.; Dupont-Gillain, C.; Demoustier-Champagne, S. Synthesis of Collagen Nanotubes with Highly Regular Dimensions through Membrane-Templated Layer-by-Layer Assembly. *Biomacromolecules* **2009**, *10*, 1021–1024.
25. Geng, Y.; Dalhaimer, P.; Cai, S.; Tsai, R.; Tewari, M.; Minko, T.; Discher, D. E. Shape Effects of Filaments *versus* Spherical Particles in Flow and Drug Delivery. *Nat. Nanotechnol.* **2007**, *2*, 249–255.
26. He, X. M.; Carter, D. C. Atomic Structure and Chemistry of Human Serum Albumin. *Nature* **1992**, *358*, 209–215.
27. Curry, S.; Mandelkow, H.; Brick, P.; Franks, N. Crystal Structure of Human Serum Albumin Complexed with Fatty Acid Reveals an Asymmetric Distribution of Binding Sites. *Nat. Struct. Biol.* **1998**, *5*, 827–835.
28. Bhattacharya, A. A.; Grüne, T.; Curry, S. Crystallographic Analysis Reveals Common Modes of Binding of Medium and Long-Chain Fatty Acids to Human Serum Albumin. *J. Mol. Biol.* **2000**, *303*, 721–732.
29. Sato, T.; Komatsu, T.; Nakagawa, A.; Tsuchida, E. Induced Long-Range Attractive Potentials of Human Serum Albumin by Ligand Binding. *Phys. Rev. Lett.* **2007**, *98*, 208101-1–208101-4.
30. Donath, E.; Sukhorukov, G. B.; Caruso, F.; Davis, S. A.; Möhwald, H. Novel Hollow Polymer Shells by Colloid-Templated Assembly of Polyelectrolytes. *Angew. Chem., Int. Ed.* **1998**, *37*, 2202–2205.
31. Dubas, S. T.; Schlenoff, J. B. Swelling and Smoothing of Polyelectrolyte Multilayers by Salt. *Langmuir* **2001**, *17*, 7725–7727.
32. Miller, M. D.; Bruening, M. L. Correlation of the Swelling and Permeability of Polyelectrolyte Multilayer Films. *Chem. Mater.* **2005**, *17*, 5375–5381.
33. Grdadolnik, J.; Maréchal, Y. Bovine Serum Albumin Observed by Infrared Spectrometry. I. Methodology, Structural Investigation, and Water Uptake. *Biopolymers* **2001**, *62*, 40–53.
34. Neault, J. F.; Tajimir-Riahi, H. A. Interaction of Cisplatin with Human Serum Albumin. Drug Binding Mode and Protein Secondary Structure. *Biochim. Biophys. Acta* **1998**, *1384*, 153–159.
35. Peters, T. *All about Albumin: Biochemistry, Genetics and Medical Applications*; Academic Press: San Diego, CA, 1996.
36. Kragh-Hansen, U. Structure and Ligand Binding Properties of Human Serum Albumin. *Dan. Med. Bull.* **1990**, *37*, 57–84.
37. Duff, M. R.; Kumar, C. V. Site-Selective Photocleavage of Proteins by Uranyl Ions. *Angew. Chem., Int. Ed.* **2006**, *45*, 137–139.
38. Tatikolov, A. S.; Costa, S. M. B. Complexation of Polymethine Dyes with Human Serum Albumin: A Spectroscopic Study. *Biophys. Chem.* **2004**, *107*, 33–49.
39. Baracca, A.; Sgarbi, G.; Solaini, G.; Lenaz, G. Rhodamine 123 as a Probe of Mitochondrial Membrane Potential: Evaluation of Proton Flux through F_0 during ATP Synthesis. *Biochim. Biophys. Acta* **2003**, *1606*, 137–146.
40. Muller-Eberhard, U.; Morgan, W. T. Porphyrin-Binding Proteins in Serum. *Ann. N.Y. Acad. Sci.* **1975**, *244*, 624–650.
41. Wardell, M.; Wang, Z.; Ho, J. X.; Robert, J.; Ruker, F.; Rubel, J.; Carter, D. C. The Atomic Structure of Human Methemalbumin at 1.9 Å. *Biochem. Biophys. Res. Commun.* **2002**, *291*, 813–819.
42. Zunszain, P. A.; Ghuman, J.; Komatsu, T.; Tsuchida, E.; Curry, S. Crystal Structural Analysis of Human Serum Albumin Complexed with Hemin and Fatty Acid. *BMC Struct. Biol.* **2003**, *3*, 6.
43. The pictures were produced on the basis of crystal structure coordinates using PyMOL. DeLano, W. L. *The PyMOL Molecular Graphics System*; DeLano Scientific: San Carlos, CA, 2002.
44. Komatsu, T.; Wang, R.-M.; Zunszain, P. A.; Curry, S.; Tsuchida, E. Photosensitized Reduction of Water to Hydrogen Using Human Serum Albumin Complexed with Zinc-Protoporphyrin IX. *J. Am. Chem. Soc.* **2006**, *127*, 16297–16301.
45. Komatsu, T.; Ohmichi, N.; Nakagawa, A.; Zunszain, P. A.; Curry, S.; Tsuchida, T. O_2 and CO Binding Properties of Artificial Hemoproteins Formed by Complexing Iron Protoporphyrin IX with Human Serum Albumin Mutants. *J. Am. Chem. Soc.* **2005**, *127*, 15933–15942.
46. Komatsu, T.; Nakagawa, A.; Zunszain, P. A.; Curry, S.; Tsuchida, E. Genetic Engineering of the Heme Pocket in Human Serum Albumin: Modulation of O_2 Binding of Iron Protoporphyrin IX by Variation of Distal Amino Acids. *J. Am. Chem. Soc.* **2007**, *129*, 11286–11295.
47. Wilchek, M.; Bayer, E. A. The Avidin−Biotin Complex in Bioanalytical Applications. *Anal. Biochem.* **1988**, *171*, 1–32.
48. Numbers of NH_2 group on fluorescence latex nanobeads are 4.75×10^4 per particle for 100 nm nanobeads and 4.02×10^5 per particle for 250 nm nanobeads, from manufacturer's quantitation.
49. Green, N. M. Spectrophotometric Determination of Avidin and Biotin. *Methods Enzymol.* **1970**, *18*, 418–424.
50. Morgan, W.; Smith, A.; Koskelo, P. The Interaction of Human Serum Albumin and Hemopexin with Porphyrins. *Biochim. Biophys. Acta* **1980**, *624*, 271–285.